

Cite this: *Nanoscale Adv.*, 2025, 7, 4152Received 15th February 2025  
Accepted 9th May 2025

DOI: 10.1039/d5na00155b

rsc.li/nanoscale-advances

# A melamine supported on TiO<sub>2</sub> coated Fe<sub>3</sub>O<sub>4</sub>@C nanocomposite as a bifunctional, effective and reusable catalyst for the Knoevenagel condensation reaction†

Somayeh Abaezadeh, Alireza Salimi Beni \* and Aliyeh Barzkar

In this study, a novel magnetic melamine-supported on TiO<sub>2</sub> coated Fe<sub>3</sub>O<sub>4</sub>@carbon nanocomposite with a core-shell structure (Fe<sub>3</sub>O<sub>4</sub>@C@TiO<sub>2</sub>/melamine) as a bifunctional catalyst is successfully synthesized via chemical grafting of propylmelamine groups on an Fe<sub>3</sub>O<sub>4</sub>@C@TiO<sub>2</sub> nanocomposite. The physicochemical properties of this catalyst were characterized by VSM, EDX, XRD, FT-IR, TGA and SEM techniques. The catalytic activity of Fe<sub>3</sub>O<sub>4</sub>@C@TiO<sub>2</sub>/melamine was studied in the Knoevenagel condensation of ethyl cyanoacetate with various benzaldehydes (electron-donating and electron-withdrawing groups) at 50 °C under solvent-free conditions. This catalyst was recovered and reused several times without significant decrease in efficiency and stability.

## 1. Introduction

In the past few decades, Fe<sub>3</sub>O<sub>4</sub> nanoparticles have attracted much attention from researchers due to their remarkable properties and applications in various fields such as adsorption, supported catalysis, optoelectronics, environmental remediation, and magnetic resonance imaging (MRI).<sup>1–8</sup> Despite their remarkable properties and widespread applications, Fe<sub>3</sub>O<sub>4</sub> nanoparticles face several inherent challenges that hinder their broader adoption. These issues include susceptibility to oxidation in the presence of air, a tendency towards self-assembly, and instability under alkaline and acidic conditions. To mitigate these drawbacks and enhance their functional characteristics, considerable efforts have been directed towards developing suitable organic or inorganic coatings that can effectively shield the surface of Fe<sub>3</sub>O<sub>4</sub> nanoparticles, enabling improved stability and performance for diverse applications.<sup>9</sup> Of the various organic and inorganic coating materials, carbon has garnered significant interest as a promising candidate for Fe<sub>3</sub>O<sub>4</sub> nanoparticle encapsulation. This interest stems from carbon's advantageous properties, including chemical stability across a broad pH range encompassing both acidic and alkaline conditions, as well as its resilience at elevated temperatures and pressures.<sup>10–12</sup> The Fe<sub>3</sub>O<sub>4</sub>@carbon composites exhibit potential for diverse applications, including catalyst supports,<sup>13,14</sup> adsorbents,<sup>15,16</sup> and electrodes.<sup>17</sup> The unique properties of carbon

coatings make them an attractive choice for enhancing the performance and durability of Fe<sub>3</sub>O<sub>4</sub> nanoparticles in diverse applications.

Titanium, a versatile metal, has found widespread applications in diverse chemical processes due to its non-toxic nature, cost-effectiveness, and excellent biocompatibility. Titanium dioxide (TiO<sub>2</sub>), a prominent titanium-containing compound, has garnered considerable research interest due to its unique properties. Owing to its non-toxicity, chemical stability, low cost, and other advantageous attributes, TiO<sub>2</sub> is extensively employed in chemical transformations as both a catalyst and a catalyst support.<sup>18,19</sup>

The Knoevenagel reaction is a crucial process for the synthesis of  $\alpha,\beta$ -unsaturated compounds *via* the condensation of activated methylene compounds with carbonyl compounds, typically catalyzed by alkaline species. While numerous homogeneous and heterogeneous alkaline catalysts have been employed to promote this transformation, heterogeneous catalysts have garnered significant attention due to their inherent advantages in terms of recyclability and reusability.<sup>20–22</sup> Some of the recently reported heterogeneous catalytic systems are Co-MOF/COF,<sup>23</sup> B-V-PIL/W,<sup>24</sup> chitosan,<sup>21</sup> Fe<sub>3</sub>O<sub>4</sub>@OS-NH<sub>2</sub>,<sup>25</sup> CFNPs<sup>26</sup> and MS/Ag<sub>2</sub>CO<sub>3</sub>.<sup>27</sup> Continuing this line of research, this study reports the synthesis and catalytic application of a novel magnetic, core-shell nanocomposite, melamine-supported TiO<sub>2</sub> coated on Fe<sub>3</sub>O<sub>4</sub>@carbon. This material acts as a bifunctional catalyst, leveraging the acidic properties of TiO<sub>2</sub> and the basicity of melamine. Its efficacy, catalytic activity, recyclability, and reusability in the Knoevenagel condensation reaction are thoroughly investigated.

Department of Chemistry, Faculty of Science, Yasouj University, Yasouj, 75918-74831, Iran. E-mail: salimibeni@yu.ac.ir; alirezasalimi7173291@gmail.com

† Electronic supplementary information (ESI) available. See DOI: <https://doi.org/10.1039/d5na00155b>



## 2. Experimental section

### 2.1. Preparation of $\text{Fe}_3\text{O}_4\text{@C@TiO}_2/\text{melamine}$

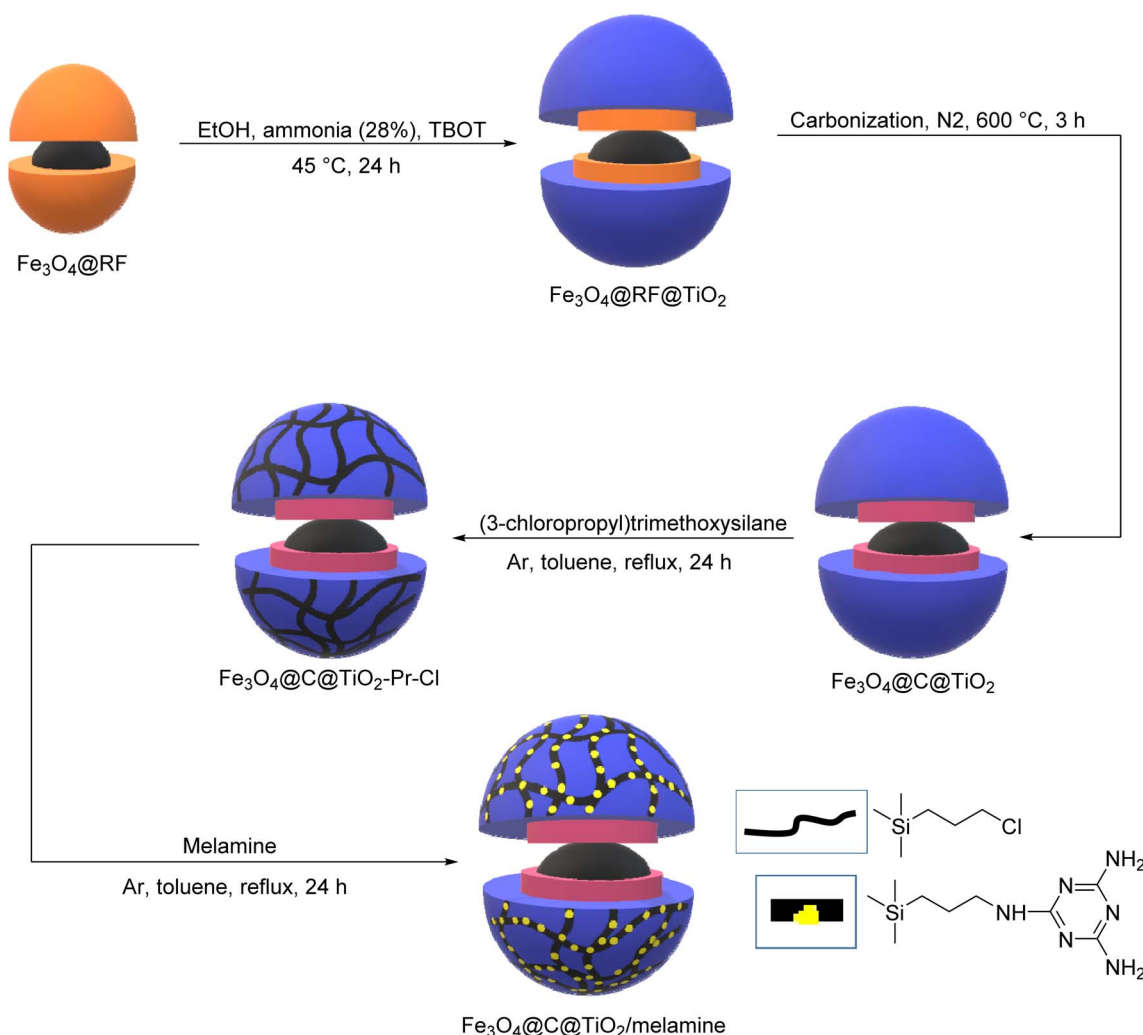
A multi-step synthesis was employed to prepare the  $\text{Fe}_3\text{O}_4\text{@C@TiO}_2/\text{melamine}$  nanocomposite. Initially,  $\text{Fe}_3\text{O}_4\text{@-resorcinol-formaldehyde}$  ( $\text{Fe}_3\text{O}_4\text{@RF}$ ) nanoparticles (NPs) were synthesized following a previously reported protocol.<sup>19</sup> Subsequently, 0.3 g of  $\text{Fe}_3\text{O}_4\text{@RF}$  NPs was dispersed in a solution of 400 mL EtOH and 1.2 mL 28% ammonia under ultrasonic agitation for 30 min. Tetrabutyl orthotitanate (TBOT, 3 mL) was then added dropwise, and the resulting mixture was stirred at 45 °C for 24 h. The synthesized product was magnetically separated, washed with EtOH, and dried at 100 °C for 6 h, yielding  $\text{Fe}_3\text{O}_4\text{@RF@TiO}_2$ .  $\text{Fe}_3\text{O}_4\text{@RF@TiO}_2$  was then carbonized under a  $\text{N}_2$  atmosphere at 600 °C for 3 h (heating rate during carbonization: 5 °C min<sup>-1</sup> and  $\text{N}_2$  flow rate: 0.2 L min<sup>-1</sup>), producing  $\text{Fe}_3\text{O}_4\text{@C@TiO}_2$ .

In the subsequent functionalization steps, 0.2 g of  $\text{Fe}_3\text{O}_4\text{@-C@TiO}_2$  was dispersed in anhydrous toluene under ultrasonic irradiation for 20 min. Under an Ar atmosphere, 0.2 mL of (3-

chloropropyl)trimethoxysilane was slowly added, and the reaction mixture was refluxed for 24 h. Following the reaction, the mixture was washed with toluene and EtOH, and the resulting product was dried at 60 °C for 12 h, designated as  $\text{Fe}_3\text{O}_4\text{@-C@TiO}_2\text{-Pr-Cl}$ . Finally, 0.2 g of  $\text{Fe}_3\text{O}_4\text{@C@TiO}_2\text{-Pr-Cl}$  was dispersed in 20 mL of anhydrous toluene under ultrasonic agitation. After 20 min, 0.06 g of melamine was introduced, and the reaction mixture was refluxed under an Ar atmosphere for 24 h. The final product,  $\text{Fe}_3\text{O}_4\text{@C@TiO}_2/\text{melamine}$ , was magnetically separated, washed with EtOH, and dried at 100 °C for 6 h.

### 2.2. General procedure for the Knoevenagel condensation reaction with the $\text{Fe}_3\text{O}_4\text{@C@TiO}_2/\text{melamine}$ catalyst

For this purpose, a reaction vessel containing the  $\text{Fe}_3\text{O}_4\text{@-C@TiO}_2/\text{melamine}$  (0.005 g, 0.6 mol%) nanocatalyst was charged with benzaldehyde (1 mmol) and ethyl cyanoacetate (1 mmol). The reaction mixture was stirred at ambient temperature, and the reaction's progress was monitored by thin-layer chromatography (TLC). Upon completion, the mixture was



Scheme 1 Synthesis of the  $\text{Fe}_3\text{O}_4\text{@C@TiO}_2/\text{melamine}$ .



filtered, and the collected solid was washed with hot ethanol. The resulting precipitate was then purified by recrystallization from ethanol.

### 2.3. $^1\text{H}$ NMR and $^{13}\text{C}$ NMR data of the Knoevenagel product

**2.3.1. (*E*)-Ethyl 2-cyano-3-(4-methoxyphenyl)acrylate (Table 2, entry 7).**  $^1\text{H}$  NMR (400 MHz, DMSO):  $\delta$  (ppm) 1.43 (t, 3H,  $J$  = 7.0 Hz), 3.51 (s, 3H), 4.41 (q, 2H), 7.33 (d, 2H,  $J$  = 8.4 Hz), 7.84 (d, 2H,  $J$  = 8.4 Hz), 8.45 (s, 1H).  $^{13}\text{C}$  NMR (100 MHz, DMSO):  $\delta$  (ppm) 14.2, 39.9, 56.6, 62.0, 113.0, 120.9, 121.0, 129.3, 137.7, 156.1, 159.8.

## 3. Results and discussion

Initially,  $\text{Fe}_3\text{O}_4$ @RF NPs were synthesized following a previously reported procedure.<sup>19</sup> Subsequently, a  $\text{TiO}_2$  shell was deposited onto the  $\text{Fe}_3\text{O}_4$ @RF nanoparticles using TBOT as a precursor. Carbonization of the RF layer yielded  $\text{Fe}_3\text{O}_4$ @C@ $\text{TiO}_2$ . The surface of the  $\text{Fe}_3\text{O}_4$ @C@ $\text{TiO}_2$  material was then functionalized with (3-chloropropyl)trimethoxysilane. Finally, melamine was immobilized onto the  $\text{Fe}_3\text{O}_4$ @C@ $\text{TiO}_2$ -Pr-Cl, resulting in the  $\text{Fe}_3\text{O}_4$ @C@ $\text{TiO}_2$ /melamine nanocatalyst (Scheme 1).

The physicochemical properties of the  $\text{Fe}_3\text{O}_4$ @C@ $\text{TiO}_2$ /melamine nanocatalyst were evaluated by various techniques. As can be seen in Fig. 1, for all nanomaterials, the FT-IR spectrum shows a major characteristic peak at  $570\text{ cm}^{-1}$ , which is assigned to the Fe–O stretching vibrations in the  $\text{Fe}_3\text{O}_4$  particles (Fig. 1a–d). The peaks which are apperceived at 1418 and  $1621\text{ cm}^{-1}$  for  $\text{Fe}_3\text{O}_4$ @RF and  $\text{Fe}_3\text{O}_4$ @RF@ $\text{TiO}_2$  correspond to the stretching vibration of the C=C bonds in resorcinol-formaldehyde (RF) (Fig. 1a and b).<sup>19</sup> In Fig. 1d, the signals at  $3490\text{ cm}^{-1}$ ,  $1630\text{ cm}^{-1}$  and  $1560\text{ cm}^{-1}$  are attributed to  $\text{NH}_2$ , C=N and C–N bonds of melamine rings, respectively. Furthermore, for  $\text{Fe}_3\text{O}_4$ @C@ $\text{TiO}_2$ /melamine, the peaks that appeared at  $2951\text{ cm}^{-1}$  are attributed to aliphatic C–H vibrations of the propyl group (Fig. 1d).<sup>28</sup> These data confirm the successful formation of the  $\text{Fe}_3\text{O}_4$ @C@ $\text{TiO}_2$ /melamine nanocatalyst.

The EDX diagram of the  $\text{Fe}_3\text{O}_4$ @C@ $\text{TiO}_2$ -melamine nanocatalyst shows the presence of Fe, C, N, O and Ti elements in this catalyst (Fig. 2). The EDX mapping analysis also showed a uniform distribution of these elements in the nanocatalyst framework (Fig. 3). The presence of these elements confirms the successful formation of the  $\text{TiO}_2$  and carbon shells, and the successful immobilization of melamine moieties on the  $\text{TiO}_2$  shell.

The SEM image of  $\text{Fe}_3\text{O}_4$ @C@ $\text{TiO}_2$ /melamine was obtained to investigate its morphology. The SEM image demonstrated spherical nanoparticles for the  $\text{Fe}_3\text{O}_4$ @C@ $\text{TiO}_2$ /melamine nanocatalyst (Fig. 4). Furthermore, according to the histogram of the SEM image (Fig. 5), the average particle size of the  $\text{Fe}_3\text{O}_4$ @C@ $\text{TiO}_2$ /melamine nanocatalyst was  $65 \pm 2\text{ nm}$ .

The XRD patterns of  $\text{Fe}_3\text{O}_4$  and  $\text{Fe}_3\text{O}_4$ @C@ $\text{TiO}_2$ /melamine nanomaterials are shown in Fig. 6. As shown, for both samples, six characteristic peaks are observed at  $2\theta$  of 30, 35, 43, 53, 57 and 63 degree, corresponding to the crystal planes of (220), (311), (400), (422), (511) and (440), respectively. These are related to the crystalline structure of magnetite NPs confirming

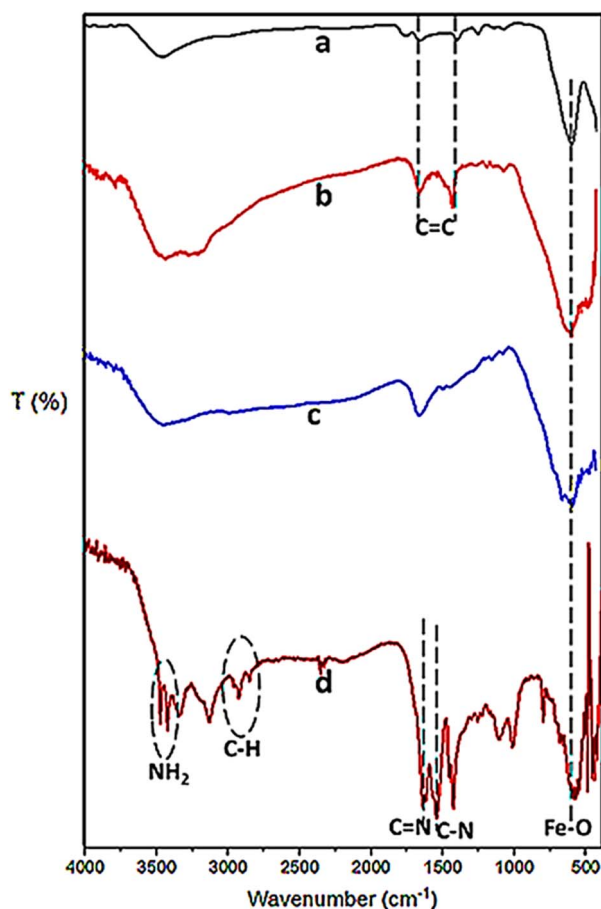


Fig. 1 FT-IR spectra of (a)  $\text{Fe}_3\text{O}_4$ @RF, (b)  $\text{Fe}_3\text{O}_4$ @RF@ $\text{TiO}_2$ , (c)  $\text{Fe}_3\text{O}_4$ @C@ $\text{TiO}_2$  and (d)  $\text{Fe}_3\text{O}_4$ @C@ $\text{TiO}_2$ -melamine.

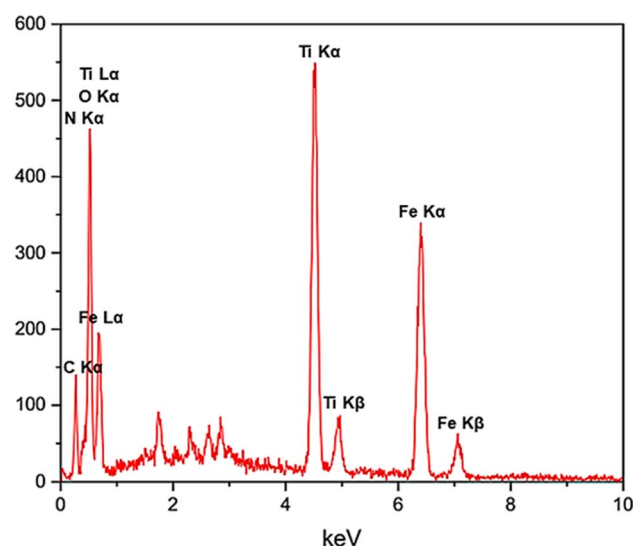


Fig. 2 EDX spectrum of the  $\text{Fe}_3\text{O}_4$ @C@ $\text{TiO}_2$ /melamine nanocatalyst.





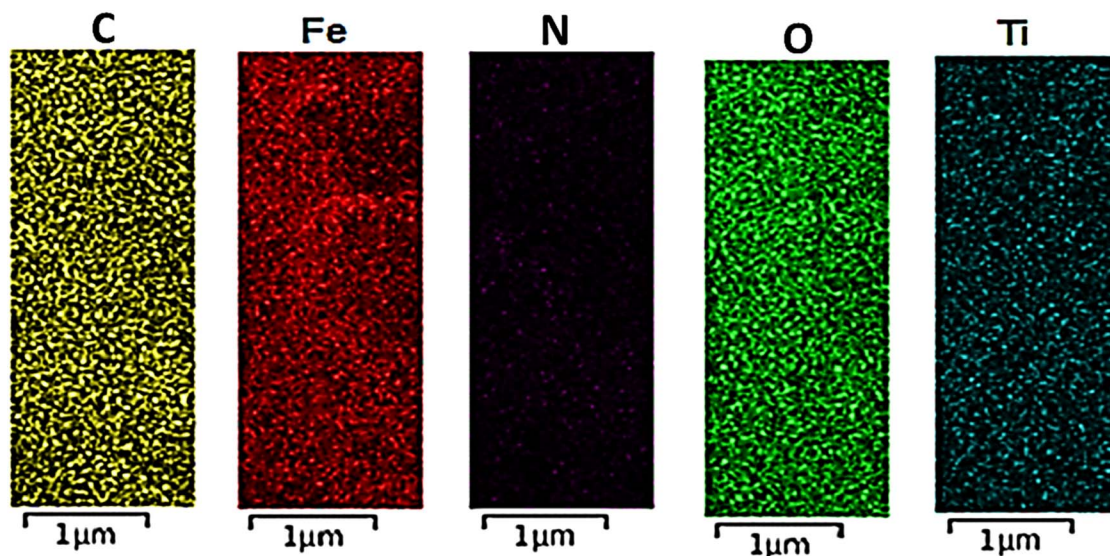


Fig. 3 EDX mapping of the  $\text{Fe}_3\text{O}_4@\text{C}@\text{TiO}_2/\text{melamine}$  nanocatalyst.

the high stability of  $\text{Fe}_3\text{O}_4$  during carbonization and catalyst preparation. As seen in Fig. 6b, the XRD pattern of the  $\text{Fe}_3\text{O}_4@\text{C}@\text{TiO}_2/\text{melamine}$  nanocatalyst confirms that the  $\text{TiO}_2$  shell on the  $\text{Fe}_3\text{O}_4$  shell was successfully formed. These results are fully consistent with previously published research.<sup>29</sup>

The magnetic properties of  $\text{Fe}_3\text{O}_4$  NPs and  $\text{Fe}_3\text{O}_4@\text{C}@\text{TiO}_2/\text{melamine}$  nanocatalyst were studied by VSM analysis. As can be seen in Fig. 7, the two materials exhibit superparamagnetic behavior without hysteresis, remanence, and coercivity. This observation confirms that the magnetic behavior of  $\text{Fe}_3\text{O}_4$  has

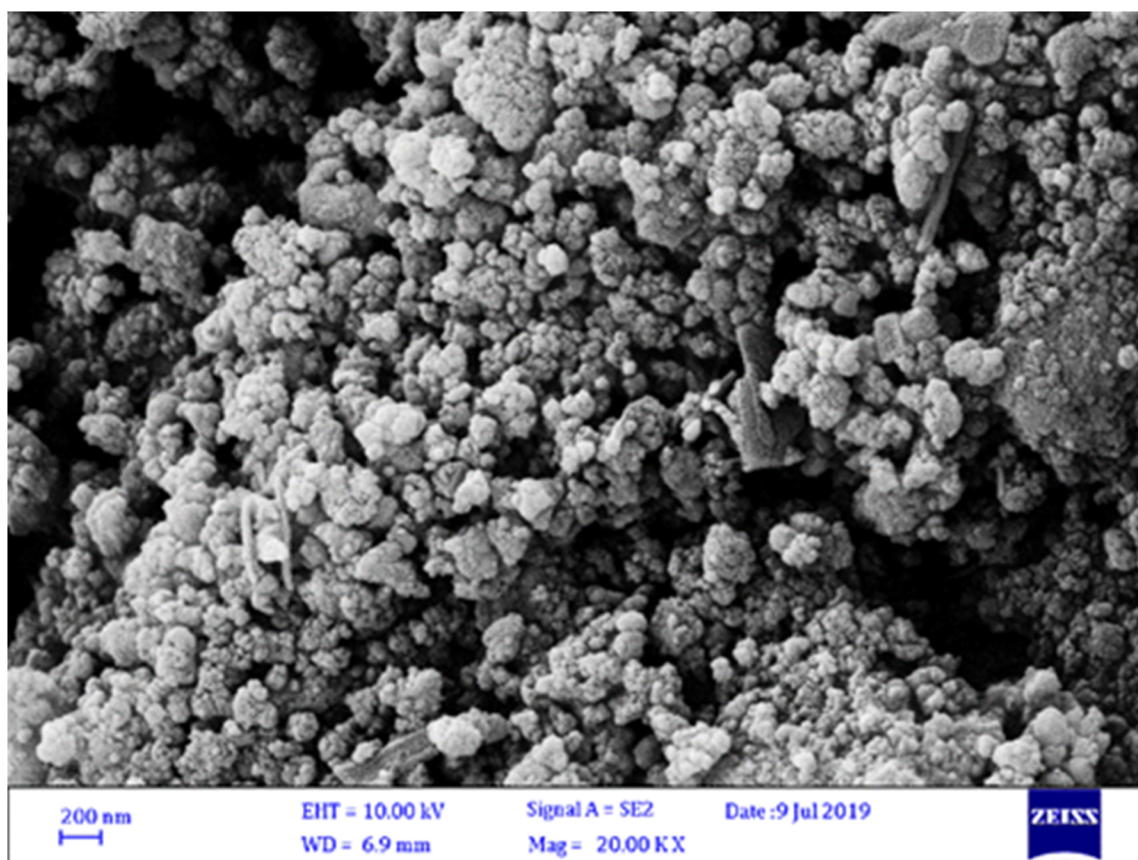


Fig. 4 The SEM image of the  $\text{Fe}_3\text{O}_4@\text{C}@\text{TiO}_2/\text{melamine}$  nanocatalyst.



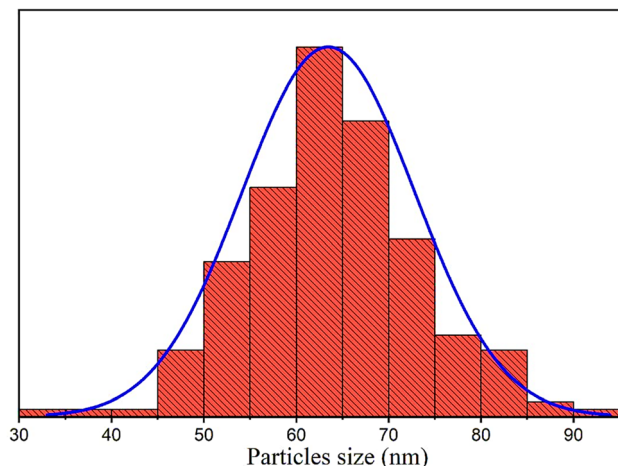


Fig. 5 The histogram of the  $\text{Fe}_3\text{O}_4@\text{C}@\text{TiO}_2/\text{melamine}$  nanocatalyst.

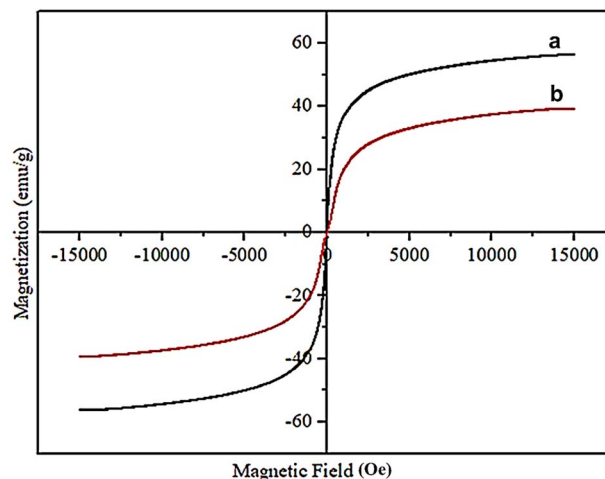


Fig. 7 VSM of (a)  $\text{Fe}_3\text{O}_4$  and (b)  $\text{Fe}_3\text{O}_4@\text{C}@\text{TiO}_2/\text{melamine}$ .

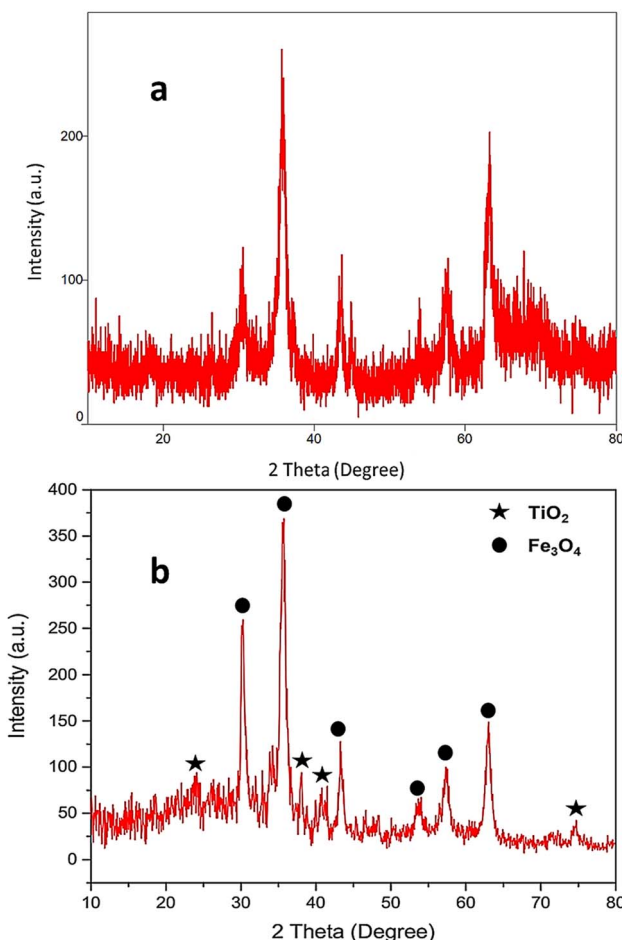


Fig. 6 XRD patterns of (a)  $\text{Fe}_3\text{O}_4$  and (b)  $\text{Fe}_3\text{O}_4@\text{C}@\text{TiO}_2/\text{melamine}$ .

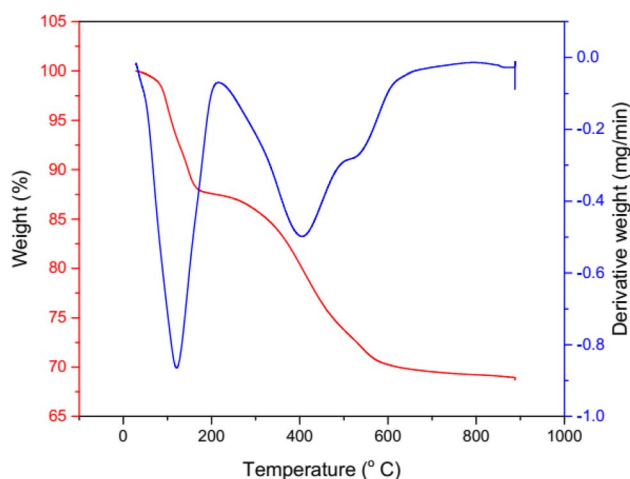


Fig. 8 TGA pattern of  $\text{Fe}_3\text{O}_4@\text{C}@\text{TiO}_2/\text{melamine}$ .

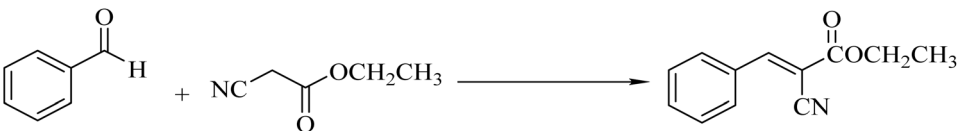
carbon and  $\text{TiO}_2$  shells and the successful chemical immobilization of the melamine moieties on  $\text{Fe}_3\text{O}_4$ .

The thermal stability of the  $\text{Fe}_3\text{O}_4@\text{C}@\text{TiO}_2/\text{melamine}$  nanocatalyst was investigated using TGA (Fig. 8). The analysis was conducted over a temperature range of 25–900 °C. An initial mass loss of approximately 10% below 200 °C is attributed to the desorption of adsorbed water and residual organic solvents from the catalyst synthesis process. A subsequent mass loss of approximately 15% between 200 and 600 °C suggests the decomposition and removal of the supported propylmelamine species. The TGA profile indicates a high degree of thermal stability for the  $\text{Fe}_3\text{O}_4@\text{C}@\text{TiO}_2/\text{melamine}$  nanocatalyst.

The catalytic activity of the synthesized and characterized  $\text{Fe}_3\text{O}_4@\text{C}@\text{TiO}_2/\text{melamine}$  catalyst was evaluated in the Knoevenagel condensation reaction. Benzaldehyde and ethyl cyanoacetate were selected as model reactants. Optimization of the reaction conditions was performed by investigating the influence of catalyst loading, temperature, and solvent (Table 1). Initially, the impact of catalyst loading on reaction progression

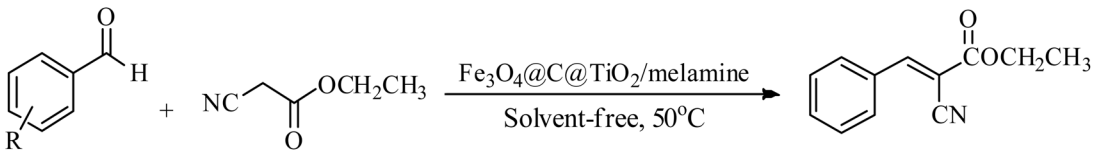
not changed after the high-temperature carbonization process. Furthermore, the magnetic saturation of  $\text{Fe}_3\text{O}_4$  is  $\sim 50$  and the magnetic saturation of  $\text{Fe}_3\text{O}_4@\text{C}@\text{TiO}_2/\text{melamine}$  is  $\sim 30$ . The decrease in the magnetic saturation of  $\text{Fe}_3\text{O}_4@\text{C}@\text{TiO}_2/\text{melamine}$  relative to  $\text{Fe}_3\text{O}_4$  confirms the successful formation of



Table 1 The effect of solvent, temperature, and catalyst loading in the Knoevenagel condensation<sup>a</sup>


Entry	Catalyst	Catalyst (mol%)	Time (min)	Temperature (°C)	Solvent	Yield <sup>b</sup> (%)
1	—	—	20	50	—	Trace
2	Fe <sub>3</sub> O <sub>4</sub> @C@TiO <sub>2</sub> /melamine	0.1	20	50	—	30
3	Fe <sub>3</sub> O <sub>4</sub> @C@TiO <sub>2</sub> /melamine	0.3	20	50	—	45
4	<b>Fe<sub>3</sub>O<sub>4</sub>@C@TiO<sub>2</sub>/melamine</b>	<b>0.6</b>	<b>20</b>	<b>50</b>	—	<b>95</b>
5	Fe <sub>3</sub> O <sub>4</sub> @C@TiO <sub>2</sub> /melamine	0.7	20	50	—	95
6	Fe <sub>3</sub> O <sub>4</sub> @C@TiO <sub>2</sub> /melamine	0.8	20	50	—	95
7	Fe <sub>3</sub> O <sub>4</sub> @C@TiO <sub>2</sub> /melamine	0.6	20	r.t.	—	70
8	Fe <sub>3</sub> O <sub>4</sub> @C@TiO <sub>2</sub> /melamine	0.6	20	60	—	95
9	Fe <sub>3</sub> O <sub>4</sub> @C@TiO <sub>2</sub> /melamine	0.6	20	50	H <sub>2</sub> O	80
10	Fe <sub>3</sub> O <sub>4</sub> @C@TiO <sub>2</sub> /melamine	0.6	20	50	EtOH	70
11	Fe <sub>3</sub> O <sub>4</sub> @C@TiO <sub>2</sub> /melamine	0.6	20	50	MeOH	75
12	Fe <sub>3</sub> O <sub>4</sub> @C@TiO <sub>2</sub> /melamine	0.6	20	50	CH <sub>3</sub> CN	40
13	TiO <sub>2</sub>	0.005 g	20	50	—	20
14	Melamine	0.005 g	20	50	—	52

<sup>a</sup> Conditions of reaction: ethyl cyanoacetate (1 mmol) and benzaldehyde (1 mmol). <sup>b</sup> Isolated yield.

Table 2 Knoevenagel condensation of ethyl cyanoacetate with various aldehydes using the Fe<sub>3</sub>O<sub>4</sub>@C@TiO<sub>2</sub>/melamine nanocatalyst<sup>a</sup>


Entry	Aldehyde	Time (min)	Yield <sup>b</sup> (%)	Mp (°C)	Ref.
1	PhCHO	20	95	51–53	25
2	3-NO <sub>2</sub> -PhCHO	10	92	163–165	30
3	4-Br-PhCHO	12	90	88–90	27
4	4-Cl-PhCHO	15	96	88–90	25
5	4-Me-PhCHO	18	88	98–100	25
6	2-Me-PhCHO	18	87	66–68	30
7	4-OMe-PhCHO	20	85	79–81	30
8	4-OH-PhCHO	25	88	169–171	25
9	4-NO <sub>2</sub> -PhCHO	10	92	173–175	25

<sup>a</sup> Conditions of reaction: ethyl cyanoacetate (1 mmol), aldehyde (1 mmol), Fe<sub>3</sub>O<sub>4</sub>@C@TiO<sub>2</sub>/melamine (0.6 mol%), 50 °C. <sup>b</sup> Isolated yields.

was assessed. The necessity of the catalyst for the reaction to proceed was confirmed. A catalyst loading of 0.6 mol% Fe<sub>3</sub>O<sub>4</sub>@C@TiO<sub>2</sub>/melamine was determined to be optimal (Table 1, entries 1–6). Subsequently, the effect of temperature was investigated, with the highest conversion observed at 50 °C (Table 1, entry 4 vs. entries 7 and 8). The influence of solvent was explored through a comparative study. Solvent-free conditions yielded the highest product formation. The use of polar protic and aprotic solvents (H<sub>2</sub>O, EtOH, MeOH, and CH<sub>3</sub>CN) resulted in diminished performance. This reduction in activity is likely

attributable to hydrogen bond formation between the solvent molecules and the melamine functional groups on the catalyst surface, which may hinder substrate access or catalyst activation (Table 1, entry 4 vs. entries 9–12). Based on these results, the optimized reaction conditions were determined to be 0.6 mol% catalyst loading, a temperature of 50 °C, and solvent-free conditions. To elucidate the synergistic effects of TiO<sub>2</sub> and melamine on the catalytic activity, the performance of the Fe<sub>3</sub>O<sub>4</sub>@C@TiO<sub>2</sub>/melamine catalyst was compared with individual TiO<sub>2</sub> and melamine counterparts (Table 1, entry 4 vs. entries 13





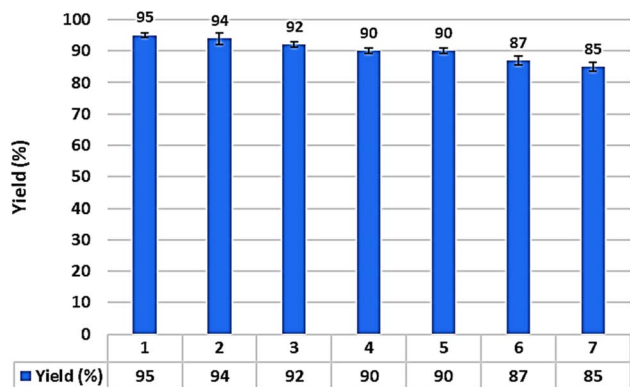


Fig. 9 Recoverability results of the  $\text{Fe}_3\text{O}_4@\text{C}@\text{TiO}_2/\text{melamine}$  catalyst.

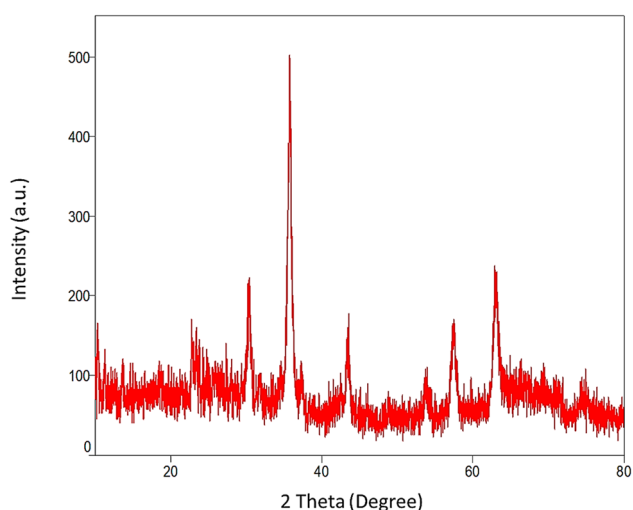


Fig. 10 PXRD pattern of the recovered  $\text{Fe}_3\text{O}_4@\text{C}@\text{TiO}_2/\text{melamine}$  catalyst.

and 14). The results revealed that  $\text{TiO}_2$  and melamine alone yielded only low to moderate product formation. In contrast, the  $\text{Fe}_3\text{O}_4@\text{C}@\text{TiO}_2/\text{melamine}$  catalyst exhibited superior catalytic activity, suggesting a synergistic interaction between the  $\text{TiO}_2$  and melamine components. These findings corroborate the hypothesis that both  $\text{TiO}_2$  and melamine are crucial for facilitating the reaction progression. Thus, it can be concluded that the  $\text{Fe}_3\text{O}_4@\text{C}@\text{TiO}_2/\text{melamine}$  catalyst functions as a bifunctional system, where the individual components cooperate to enhance the overall catalytic performance.

Having established the optimal reaction parameters (Table 1, entry 4), the Knoevenagel condensation was explored using a diverse range of aromatic aldehydes (Table 2). Irrespective of the electronic properties or substitution patterns of the aromatic aldehydes, the presence of electron-withdrawing or electron-donating substituents had negligible impact on the reaction efficiency. The  $\text{Fe}_3\text{O}_4@\text{C}@\text{TiO}_2/\text{melamine}$  catalytic system consistently demonstrated a high to excellent yield of the desired Knoevenagel products, highlighting the versatility

and efficacy of this catalytic system. It is noteworthy that, according to previous studies, the condensation of cyanoacetate with both aromatic and aliphatic aldehydes yields the *E*-isomer, with no formation of by-products.<sup>27</sup>

A leaching test was conducted to assess the heterogeneous nature of the  $\text{Fe}_3\text{O}_4@\text{C}@\text{TiO}_2/\text{melamine}$  catalyst under the optimized reaction conditions described in Section 2.2. After allowing the reaction to progress to approximately 50% completion, the catalyst was separated from the reaction mixture. Upon further monitoring, no additional conversion was observed in the absence of the catalyst after 1 h, substantiating the heterogeneous character of the  $\text{Fe}_3\text{O}_4@\text{C}@\text{TiO}_2/\text{melamine}$  catalyst. This result confirms that the catalyst maintains its stability and efficacy in facilitating the desired reaction without leaching into the reaction medium, thereby demonstrating its robustness as a heterogeneous catalyst.

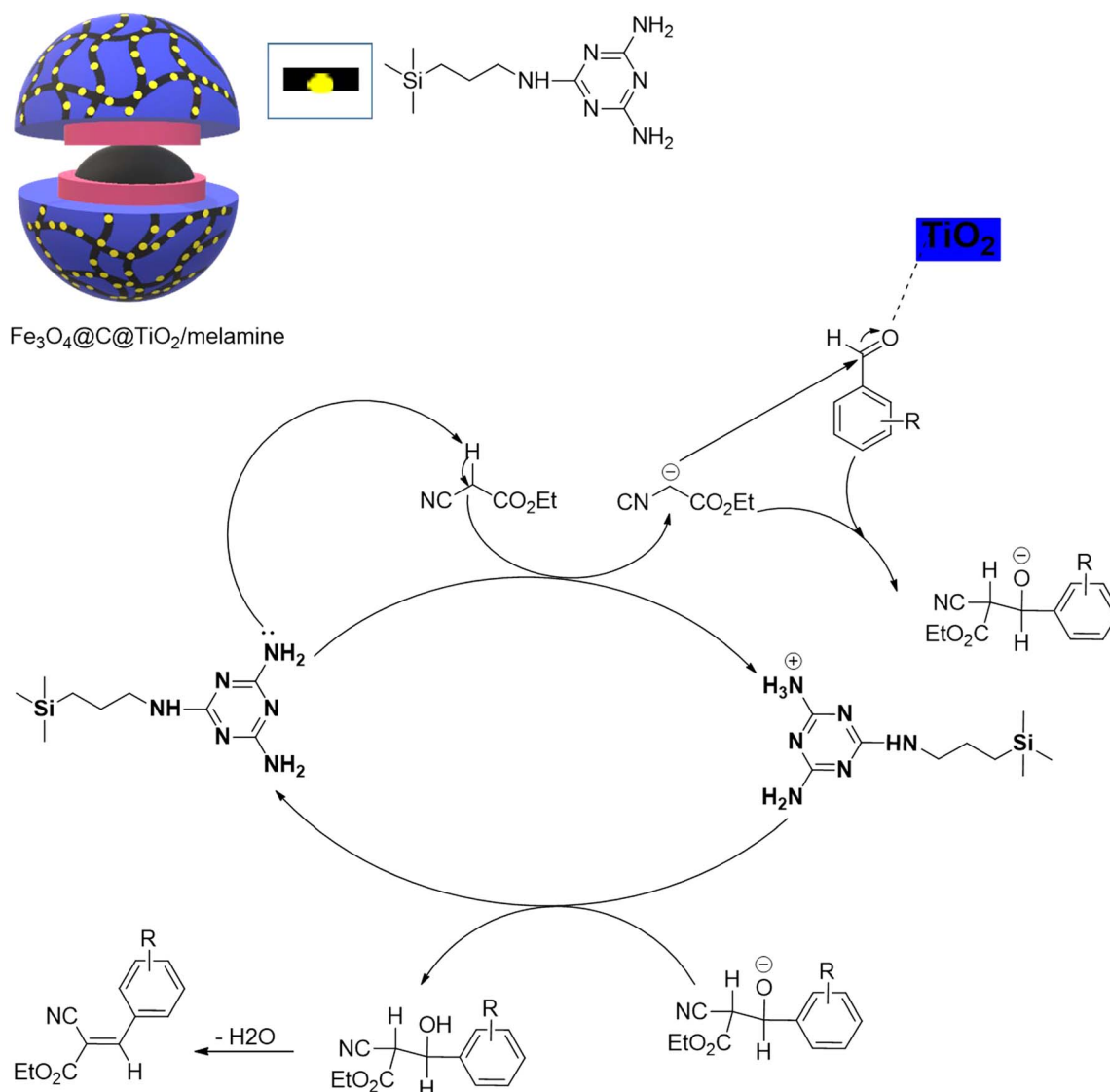
To evaluate the recyclability and stability of the  $\text{Fe}_3\text{O}_4@\text{C}@\text{TiO}_2/\text{melamine}$  nanocatalyst, a sequential study was conducted under the optimized conditions detailed in Section 2.2. The condensation reaction between benzaldehyde and ethyl cyanoacetate served as the model system. Following the completion of each reaction cycle, the nanocatalyst was conveniently recovered through magnetic separation and subsequently reused. The results (Fig. 9) demonstrated that the  $\text{Fe}_3\text{O}_4@\text{C}@\text{TiO}_2/\text{melamine}$  nanocatalyst could be effectively recycled at least six times without significant loss in its catalytic performance, thereby highlighting its durability and potential for practical applications in sustainable synthesis.

Then, the chemical and structural stability of the recovered  $\text{Fe}_3\text{O}_4@\text{C}@\text{TiO}_2/\text{melamine}$  catalyst were investigated by using XRD analysis. As shown in Fig. 10, the intensity and the position of the peaks in the XRD pattern of the recovered catalyst are in good agreement with the XRD pattern of the fresh catalyst. This analysis confirmed the stability of the crystalline structure of  $\text{Fe}_3\text{O}_4$  nanoparticles during six reuse stages.

Although the precise mechanism of the Knoevenagel condensation reaction catalyzed by  $\text{Fe}_3\text{O}_4@\text{C}@\text{TiO}_2/\text{melamine}$  remains elusive, a plausible mechanism is proposed in Scheme 2. The mechanism commences with the deprotonation of cyanoacetate by the amine functionalities present in the catalyst, resulting in the generation of the corresponding enolate species. Subsequently, the enolate undergoes a nucleophilic attack on the carbonyl carbon of the aldehyde, followed by the recapture of a proton from the protonated catalyst. This sequence of events leads to the formation of  $\beta$ -hydroxyl compounds. Finally, the desired Knoevenagel products are obtained *via* a dehydration step involving the elimination of water from the  $\beta$ -hydroxyl compounds, thus completing the catalytic cycle.<sup>25</sup>

In the latest study, the effectiveness of  $\text{Fe}_3\text{O}_4@\text{C}@\text{TiO}_2/\text{melamine}$  was compared to several new catalysts reported in the Knoevenagel condensation (Table 3). This demonstrated that  $\text{Fe}_3\text{O}_4@\text{C}@\text{TiO}_2/\text{melamine}$  is comparable to or better than most previous investigations (time or solvent). These results prove significantly the high efficacy of  $\text{Fe}_3\text{O}_4@\text{C}@\text{TiO}_2/\text{melamine}$  in the Knoevenagel condensation.





Scheme 2 Proposed mechanism for the Knoevenagel condensation using the  $\text{Fe}_3\text{O}_4@\text{C}@\text{TiO}_2/\text{melamine}$  catalyst.

**Table 3** Comparative investigation of the efficacy of  $\text{Fe}_3\text{O}_4@\text{C}@\text{TiO}_2/\text{melamine}$  with that of the previously reported catalytic system in the Knoevenagel reaction

Catalyst	Solvent	Temperature (°C)	Time (min)	Yield (%)	Ref.
CNT-g-PDMAEMA/ $\text{Fe}_3\text{O}_4$ NPs (80 mg)	Water	Reflux	360	99.2	31
$\text{Fe}_3\text{O}_4$ -PPCA nanoparticles (0.5 g)	$\text{CH}_2\text{Cl}_2$	25	120	92	32
Aminofunctionalized MCM-48 and SBA-15 (1.5 mol%)	Benzene	25	75	100	33
$\text{Fe}_3\text{O}_4@\text{C}@\text{MCM}41$ -guanidine (1.5 mol%)	Solvent-free	RT	90	98	34
$\text{Fe}_3\text{O}_4@\text{SiO}_2@\text{CuO}-\text{Fe}_2\text{O}_3$ (0.03 g)	Water	Reflux	7	91	35
MNPs-guanidine (0.005 g, 0.39 mol%)	PEG/ $\text{H}_2\text{O}$	25	150	96	36
$\text{Fe}_3\text{O}_4@\text{C}@\text{TiO}_2/\text{melamine}$ (0.6 mol%)	Solvent-free	50	20	95	This work

## 4. Conclusion

In this research, a novel magnetic core-shell nanocomposite catalyst comprised of melamine supported on  $\text{TiO}_2$ -coated

$\text{Fe}_3\text{O}_4$ @carbon was synthesized and characterized. The successful incorporation of the catalytic components within the material framework was confirmed through comprehensive characterization techniques, including FT-IR, TGA, and EDX analyses. The





XRD method validated the crystalline structure of the magnetic nanoparticles. Furthermore, VSM analysis revealed the superior magnetic properties of the nanocatalyst, and SEM imaging confirmed its uniform spherical morphology. The catalytic performance of  $\text{Fe}_3\text{O}_4@\text{C}@\text{TiO}_2/\text{melamine}$  was studied using the Knoevenagel condensation of ethyl cyanoacetate and various benzaldehydes bearing electron-donating and electron-withdrawing substituents. Notably, the catalyst displayed exceptional stability, enabling its recycling and reuse for at least six reaction cycles without significant loss in efficiency.

## Data availability

All data and materials are included in the manuscript.

## Author contributions

S. A.: writing – original draft, investigation, resources, formal analysis. A. S. B.: conceptualization, writing – review & editing, supervision, visualization. A. B.: writing – original draft, formal analysis.

## Conflicts of interest

There are no conflicts of interest to declare.

## Acknowledgements

The authors thank the Yasouj University for supporting this work.

## References

- 1 A. H. Lu, E. e. L. Salabas and F. Schüth, *Angew. Chem., Int. Ed.*, 2007, **46**, 1222–1244.
- 2 M. B. Gawande, A. K. Rath, I. D. Nogueira, R. S. Varma and P. S. Branco, *Green Chem.*, 2013, **15**, 1895–1899.
- 3 M. B. Gawande, P. S. Branco and R. S. Varma, *Chem. Soc. Rev.*, 2013, **42**, 3371–3393.
- 4 M. B. Gawande, V. D. Bonifácio, R. S. Varma, I. D. Nogueira, N. Bundaleski, C. A. A. Ghumman, O. M. Teodoro and P. S. Branco, *Green Chem.*, 2013, **15**, 1226–1231.
- 5 S. Zeng, D. Baillargeat, H.-P. Ho and K.-T. Yong, *Chem. Soc. Rev.*, 2014, **43**, 3426–3452.
- 6 S. Delice, M. Isik and N. Gasanly, *Chem. Phys. Lett.*, 2024, **840**, 141139.
- 7 P. Goyal, S. Chakraborty and S. K. Misra, *Environ. Nanotechnol., Monit. Manage.*, 2018, **10**, 28–35.
- 8 S. Xuan, F. Wang, J. M. Lai, K. W. Sham, Y.-X. J. Wang, S.-F. Lee, J. C. Yu, C. H. Cheng and K. C.-F. Leung, *ACS Appl. Mater. Interfaces*, 2011, **3**, 237–244.
- 9 M. Shaker and D. Elhamifar, *Front. Energy Res.*, 2020, **8**, 78.
- 10 L. Ren, H. Lin, F. Meng and F. Zhang, *Ceram. Int.*, 2019, **45**, 9646–9652.
- 11 J. Wang, H.-Y. Tan, M.-Y. Qi, J.-Y. Li, Z.-R. Tang, N.-T. Suen, Y.-J. Xu and H. M. Chen, *Chem. Soc. Rev.*, 2023, **52**, 5013–5050.
- 12 X.-J. Li, H.-T. Wan, M.-Y. Qi, C.-L. Tan and Z.-R. Tang, *Mol. Catal.*, 2024, **564**, 114356.
- 13 Q. An, M. Yu, Y. Zhang, W. Ma, J. Guo and C. Wang, *J. Phys. Chem. C*, 2012, **116**, 22432–22440.
- 14 Y. Wang, H. Sun, H. M. Ang, M. O. Tadé and S. Wang, *Chem. Eng. J.*, 2014, **245**, 1–9.
- 15 R.-S. Juang, Y.-C. Yei, C.-S. Liao, K.-S. Lin, H.-C. Lu, S.-F. Wang and A.-C. Sun, *J. Taiwan Inst. Chem. Eng.*, 2018, **90**, 51–60.
- 16 Z. Zhang and J. Kong, *J. Hazard. Mater.*, 2011, **193**, 325–329.
- 17 H. Fan, R. Niu, J. Duan, W. Liu and W. Shen, *ACS Appl. Mater. Interfaces*, 2016, **8**, 19475–19483.
- 18 L. Oi, M. Choo, H. Lee, H. Ong, S. Hamid and J. Juan, *RSC Adv.*, 2016, **6**, 108741–108754.
- 19 A. Barzkar, A. S. Beni, S. Abaezadeh and S. Parang, *Results Chem.*, 2024, **8**, 101599.
- 20 J. N. Appaturi, R. Ratti, B. L. Phoon, S. M. Batagarawa, I. U. Din, M. Selvaraj and R. J. Ramalingam, *Dalton Trans.*, 2021, **50**, 4445–4469.
- 21 B. Sakthivel and A. Dhakshinamoorthy, *J. Colloid Interface Sci.*, 2017, **485**, 75–80.
- 22 J. Ortiz-Bustos, P. Cruz, Y. Pérez and I. del Hierro, *Mol. Catal.*, 2022, **524**, 112328.
- 23 E. Rahmati and Z. Rafiee, *J. Porous Mater.*, 2021, **28**, 19–27.
- 24 N. Abedian-Dehaghani, S. Sadjadi and M. M. Heravi, *Sci. Rep.*, 2022, **12**, 16395.
- 25 R. Mirbagheri, D. Elhamifar and M. Norouzi, *New J. Chem.*, 2018, **42**, 10741–10750.
- 26 A. Mishra, P. Yadav and S. K. Awasthi, *ACS Org. Inorg. Au*, 2023, **3**, 254–265.
- 27 F. Karimkhah, D. Elhamifar and M. Shaker, *Sci. Rep.*, 2021, **11**, 18736.
- 28 Z. Haydari, D. Elhamifar, M. Shaker and M. Norouzi, *Appl. Surf. Sci. Adv.*, 2021, **5**, 100096.
- 29 A. Wojciechowska, A. Markowska-Szczupak and Z. Lendzion-Bieluń, *Materials*, 2022, **15**, 1863.
- 30 D. Elhamifar, S. Kazempoor and B. Karimi, *Catal. Sci. Technol.*, 2016, **6**, 4318–4326.
- 31 L. Geng, Y. Tian, R. Ding, C. Zhao, Q. Shi and H. Xu, *Colloids Surf., A*, 2024, **685**, 133283.
- 32 E. Karaoğlu, A. Baykal, M. Şenel, H. Sözeri and M. S. Toprak, *Mater. Res. Bull.*, 2012, **47**, 2480–2486.
- 33 N. T. Phan and C. W. Jones, *J. Mol. Catal. A: Chem.*, 2006, **253**, 123–131.
- 34 A. Barzkar and A. S. Beni, *Sci. Rep.*, 2023, **13**, 10336.
- 35 M. Gilanizadeh and B. Zeynizadeh, *Res. Chem. Intermed.*, 2018, **44**, 6053–6070.
- 36 A. Rostami, B. Atashkar and H. Gholami, *Catal. Commun.*, 2013, **37**, 69–74.

